Saudi Dental Journal (2022) **34**, 375–384

King Saud University

Saudi Dental Journal

www.ksu.edu.sa
www.sciencedirect.com

ORIGINAL ARTICLE

Assessment of the possible ameliorative effect of curcumin nanoformulation on the submandibular salivary gland of alloxan-induced diabetes in a rat model (Light microscopic and ultrastructural study)

Maha El Shahawy [a,*], **Mona El Deeb** [b]

[a] *Associate Professor, Oral Biology Department, Faculty of Dentistry, Minia University, Egypt*
[b] *Professor, Oral Biology Department, Faculty of Oral & Dental Medicine, Future University in Egypt (FUE), Egypt*

Received 19 February 2022; revised 17 April 2022; accepted 22 April 2022
Available online 29 April 2022

KEYWORDS

Diabetes;
Nanocurcumin;
Submandibular salivary glands;
Masson trichrome;
α SMA

Abstract *Background:* Nowadays, attention is directed to herbal treatments in an attempt to lessen the adverse effects of diabetes. Nanoformulation of curcumin (NC) was shown to enhance stability and water solubility compared to native curcumin.

Objective: To examine the effect of different NC concentrations on the histopathological structure of the submandibular salivary gland of diabetic rats.

Methods: 28 rats were divided equally into 4 groups. **Group I:** Control group, **Group II** (diabetic)**, III** (diabetic + nanocurcumin low dose), and **IV** (diabetic + nanocurcumin high dose): Rats of groups II, III and IV were injected with a single dose of alloxan (140 mg/kg) to induce diabetes. After 7 days, groups III and IV were treated for 6 weeks with NC (100 mg/kg/day) for group III, and (200 mg/kg/day) for group IV. Submandibular salivary glands were assessed histologically, immunohistochemically using α smooth muscle actin (α SMA) and ultrastructurally.

Results: Diabetic samples showed destruction of parenchymal elements of the gland, with thick fiber bundles encircling the excretory ducts and minimal reaction for α SMA. Amelioration of the gland's architecture was detected in groups III and IV with reduction of collagen deposition and elevation of positive immunoreactivity to α SMA.

Conclusion: NC profoundly repaired the induced diabetic histopathological and ultrastructural alterations of the gland in a dose dependent manner.

* Corresponding author.
E-mail address: maha.elshahawy@mu.edu.eg (El Shahawy M).
Peer review under responsibility of King Saud University.

Production and hosting by Elsevier

1. Introduction

Diabetes mellitus (DM) is a metabolic illness manifested by hyperglycemia (Aziz et al., 2019; Priyadi et al., 2019; Salem et al., 2021). Diabetic complications include retinopathy, renal failure and cardiovascular diseases (Cui et al., 2021). Several

https://doi.org/10.1016/j.sdentj.2022.04.009
1013-9052

oral drawbacks accompany diabetes as periodontitis, gingivitis, dental caries, delayed wound healing, xerostomia (Maciejczyk et al., 2017; El-sharkawy et al., 2018), and abnormalities in salivary glands' functions (Abd Elhameed, 2018).

Synthetic antidiabetic agents cause several side effects; therefore, attention was directed to herbal treatments to lessen such consequences (Gouda et al., 2019).

Curcumin was on focus in the last decade owing to its antidiabetic features (Prasad et al., 2014), as it is capable to combine with different key molecules interrelated to the pathology of this illness (Kato et al., 2017; Ye et al., 2017).

Although curcumin acquires remarkable benefits, it exhibits some criteria which reduce its bioavailability limiting its use including; fast metabolism, low degree of liquefaction, low gastrointestinal absorption, and pH degradation (Estakhri et al., 2019).

Nanoparticles of a drug are useful in targeted delivery, which hinders the destruction of surrounding normal tissues (Bansal et al., 2011). They can diffuse through the cell membrane to interact with biological systems (Potphode et al., 2018). Consequently, nanocurcumin (NC) offers superior permeability, prolonged circulation, high resistance to metabolic processes, and does not have harmful effect in elevated concentrations (Araghi et al., 2017; Ranjbar et al., 2020). NC was found to alleviate histopathological aspects and cellular degeneration in induced nephrotoxicity and hepatotoxicity in rats (Kheiripour et al., 2021; Bulboacă et al., 2021).

Based on these data, we aimed to examine the effect of different NC concentrations on the histopathological structure of the submandibular salivary gland of diabetic rats.

2. Materials & methods

2.1. Materials

2.1.1. Chemicals and treatment

- Alloxan hydrate was obtained from SDFCL (Mumbai, India) in the form of powder.
- NC powder was obtained from NanoTech Egypt for Photo-Electronics, with particle size 50 ± 5.5 nm.

2.1.2. Animals

The study was performed on 28 adult male rats, 150-200gm body weight. Rats were housed under constant day/night cycle and had access to ordinary diet and water. The investigational design was permitted by the Research Ethics Committee of Faculty of Dentistry, Minia University (Decision No.509).

2.2. Induction of DM

Induction was attained by a single intraperitoneal administration of alloxan (140 mg/kg) dissolved in 4% saline solution after 12 hrs. fasting. Following 3 days, blood samples were obtained from the tail vein of each rat for measurement of plasma glucose level using a glucometer. Rats exhibited levels above 300 mg/dL were considered diabetic. Non diabetic rats were replaced by normal rats to be induced by alloxan. Blood samples were collected weekly throughout the experimental period to ensure persistence of diabetes. (Taiema et al., 2019).

2.3. Experimental design

The animals were acclimatized upon arrival for a week, and then equally divided into four groups:

Group I (Control): Rats received distilled water, via oral gavage.

Group II (Diabetic): Rats were injected with a single dose of alloxan (140 mg/kg) dissolved in 4% saline solution, and received distilled water, via oral gavage.

Similar to group II, diabetes was induced in groups III and IV. 7 days after alloxan injection and confirmation of diabetes, diabetic rats were treated for further 6 weeks; as follows:

Group III (nanocurcumin low dose) (NLD); Group IV (nanocurcumin high dose) (NHD): Diabetic rats received nanocurcumin 100 mg/kg/day (for group III) and 200 mg/kg/day (for group IV) dissolved in distilled water, via oral gavage (Shamsi-Goushki et al., 2020).

At the end of the experiment, the rats were sacrificed by intraperitoneal injection of phenobarbital (60 mg/Kg) (Pourghasem et al., 2014).

Submandibular glands were excised from both sides and prepared for the investigation procedures.

2.4. Histopathological examination

Right submandibular gland specimens were preserved in 10% formaldehyde solution for 24 h then prepared to be stained with Hematoxylin and Eosin (H&E) for histological evaluation and Masson's Trichrome to inspect collagen fiber deposition. Positive staining of collagen appeared blue or green in color (Keirnan, 2015).

2.5. Immunohistochemical examination

Sections were processed for immunostaining with α SMA (AB-7817, abcam medical, Cambridge, MA, USA). Positive reaction appeared as brown staining in myoepithelial cells' cytoplasm (El Sadik et al., 2018).

2.6. Histomorphometric analysis

Leica microscope with digital camera and software (Leica Qwin 500) was used for image analysis. Pixels were changed into real micrometer units, then five fields were analyzed for

each sample at 400x magnification and mean values were obtained. The gland tissue was examined with reference to area% of collagen fibers' deposition and immunopositivity for α SMA.

2.7. Statistical analysis

IBM SPSS software package version 20.0. (Armonk, NY: IBM Corp) was used for data analysis. Records were tested for normality by Shapiro-Wilk test. One-way analysis of variance (ANOVA) and Tukey's post-hoc tests were utilized for comparing results. P value ≤ 0.05 presented statistically significant results.

2.8. Transmission electron microscopic (TEM) examination

Left gland specimens were divided into tiny parts and preserved in a mixture of paraformaldehyde and glutaraldehyde in cacodylate buffer to be prepared for TEM examination (Taiema et al., 2019), then photographed in a JEOL 100S (Faculty of Science, Alexandria University).

3. Results

3.1. H & E results

3.1.1. Group I

Results showed coalesced deeply basophilic seromucous acini with basally situated nuclei and well defined cellular and acinar boundaries. Strongly eosinophilic striated ducts with columnar cells, central nuclei, and basal striations were clearly identified (Fig. 1a, a′).

3.1.2. Group II

The acini appeared disorganized and spaced. Some were atrophied and collapsed with indistinct cellular and acinar boundaries. Some acinar cells showed pleomorphic and hyperchromatic nuclei, while others revealed flattened and degenerated ones. The cytoplasm appeared faintly basophilic and vacuolated. The striated ducts displayed atypical configuration with areas of fragmentation and distorted cellular and ductal outlines. Flattened or even degenerated nuclei could be recognized with absence of basal striations and areas of cytoplasmic vacuolation (Fig. 1b, b′).

3.1.3. Group III

Some acini and striated ducts showed better histological picture compared to group II. However, others appeared atrophied and deformed with pyknotic or degenerated nuclei. Some ductal cells were disfigured with flattened nuclei and partial restoration of their basal striations. Few cytoplasmic vacuolated areas were still evident (Fig. 1c, c′).

3.1.4. Group IV

Most of the acini and ducts appeared intact. The epithelial lining of acini and ducts showed uniform arrangement of cells with minimal flattened or degenerated nuclei, and hardly distinguished vacuolation. Presence of basal striations was persistent feature in this group (Fig. 1d, d′).

3.2. TEM results

3.2.1. Group I

Control group revealed pyramidal well defined shaped acinar cells with rounded basally located nucleus, which exhibited regular and well demarcated nuclear outline. Normally appearing parallel arrays of rough endoplasmic reticulum (RER) and oval mitochondria having transverse infolding cristae could be detected. Extensive electron-lucent secretory granules of variable sizes were visualized with desmosomal junctions (Fig. 2a-c).

Ductal cells exhibited centrally placed rounded nucleus and prominent nucleolus. The basal membrane showed prominent

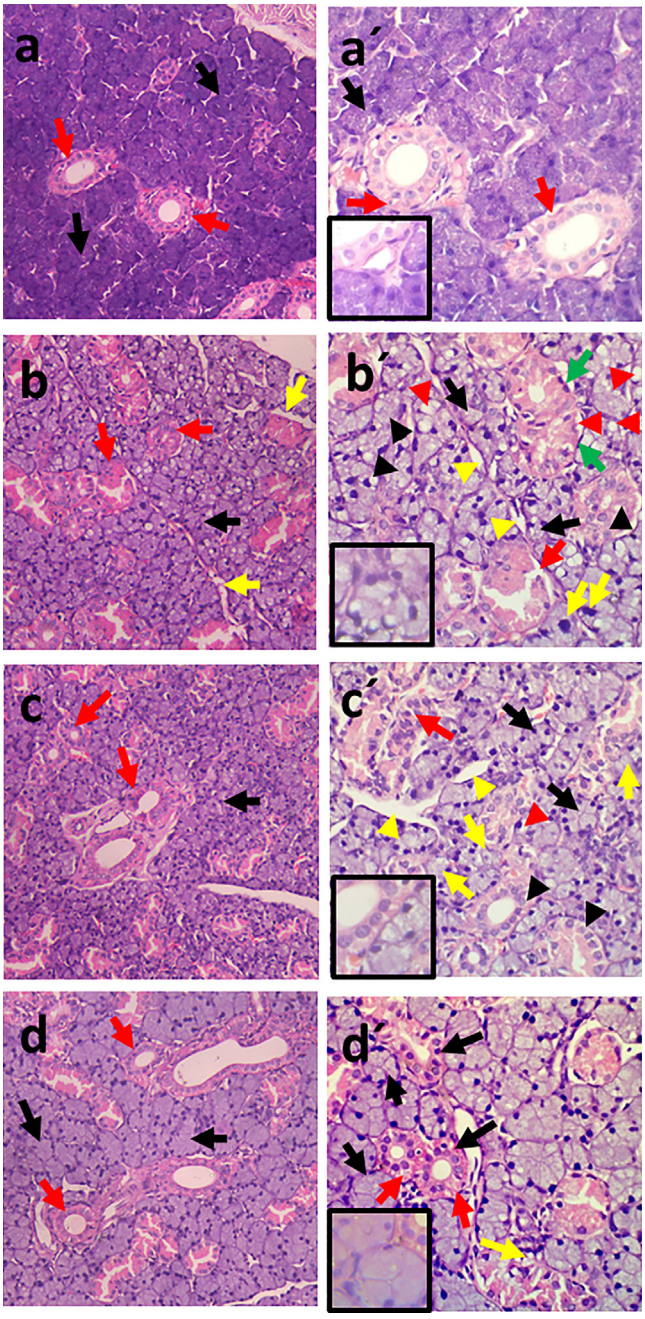

deep infoldings loaded with abundant radially arranged mitochondria displaying palisading pattern. Few scattered strands of RER were observed with numerous well circumscribed electron dense granules. Typical desmosomal junctions were also recognized (Fig. 2d-h).

3.2.2. Group II

Sections displayed noticeable atrophic changes with ill-defined shape of acinar and cellular boundaries. The nucleus showed dilated and irregular membrane indentations with perinuclear halo. Signs of cellular degeneration were evident together with intracellular cytoplasmic vacuolation. The mitochondria assumed unclear outlines with blurred cristae, while the RER appeared abnormally dilated, disrupted and fragmented. Accumulated granules were fused into large irregular membrane bounded ones with variant densities and sizes. Widened intercellular junctions with marked loss of desmosomal attachment were also spotted (Fig. 3a-d).

Striated ducts showed indistinct basal infoldings with irregular orientation. Some nuclei revealed irregularity of the nuclear membrane, others were shrunk, pyknotic and degenerated. The mitochondria appeared distended and bizarre shaped with disruption of their cristae, while the RER were disrupted and hardly distinguished. Sparse granules were evident with few desmosomal junctions and widening of intercellular spaces (Fig. 3e-h).

3.2.3. Group III

Acinar cells showed definite cellular outlines, however, few intracellular vacuolar spaces were recognized. Some nuclei displayed slight irregularity of their nuclear membrane. Uniform arrays of RER were also observed. Few mitochondria exhibited pleomorphic pattern, others were disfigured with blurred boundaries and indistinguishable cristae. Abundant granules were manifested with areas of disrupted cellular interdigitations and desmosomal junctions (Fig. 4a-c).

Fig. 1 Photomicrograph of rat submandibular gland showing: **(a) Group I; (b) Group II; (c) Group III; (d) Group IV; In figs. a, b, c, d;** basophilic seromucous acini (black arrows), eosinophilic striated ducts (red arrows). **In fig. b;** spacing between the acini (yellow arrows) (H&E x200). Higher magnification: **(a′) Group I**; well defined boundaries of acini & cells (black arrow), basal striations of striated ducts (red arrows), **(b′) Group II**; atrophied acini with indistinct boundaries (black arrows), pleomorphic and hyperchromatic nuclei of acinar cells (yellow arrows), flattened nuclei of acinar & ductal cells (green arrows), degenerated nuclei of acinar & ductal cells (black arrowheads), intracellular vacuolation (red arrowheads), disrupted outlines of striated duct (red arrows), spacing between acini (yellow arrowheads), **(c′) Group III**; normal acini (black arrows), areas of spacing (yellow arrowheads), atrophied deformed acini with degenerated nuclei (yellow arrows), disfigured striated duct (red arrow), partial restoration of basal striations (black arrowheads), intracytoplasmic vacuolation (red arrowheads), **(d′) Group IV**; uniform outlines of acini and ducts (black arrows), minimal vacuolation (yellow arrow), prominent basal striations (red arrows) (H&E x400). Insets of higher magnifications in **figs: a′, b′, c′, d′** show nuclear changes (H&E x1000).

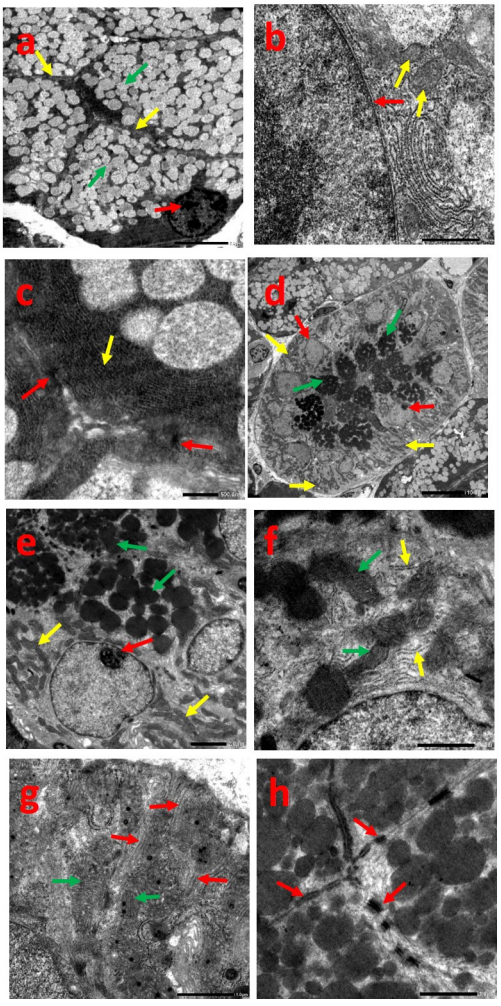

Fig. 2 Electron micrograph of group I showing: acinar cells **(a-c)**, **(a)** pyramidal acinar cells with basal nucleus (red arrow), well defined cellular boundaries (yellow arrows), electron-lucent secretory granules (green arrows), **(b)** regular & well defined nuclear outline (red arrow), mitochondria with transverse cristae (yellow arrows), **(c)** parallel arrays of RER (yellow arrow), desmosomal junctions (red arrows) (Uranyl acetate and lead citrate (a)x1500, (b)x8000, (c)x10000). Striated duct cells **(d-h)**, **(d)** columnar cells with central rounded nucleus (red arrows), basal infoldings loaded with mitochondria (yellow arrows), numerous electron dense secretory granules (green arrows), **(e)** rounded nucleus with prominent nucleolus (red arrow), well circumscribed secretory granules (green arrows), radially arranged mitochondria (yellow arrows), **(f)** elongated mitochondria with well-defined cristae (green arrows), Few scattered strands of RER (yellow arrows), **(g)** prominent deep basal infoldings (red arrows), elongated mitochondria (green arrows), **(h)** desmosomal junctions (red arrows) (Uranyl acetate and lead citrate (d)x600, (e)x2500, (f, g, h)x8000).

Few basal infoldings reappeared in the striated ducts with numerous elongated mitochondria. Regular nuclear configuration and scattered RER were identified. Secretory granules were not detected in some cells, though others expressed few of them. Intercellular junctions could be easily recognized (Fig. 4d-f).

3.2.4. Group IV

Specimens revealed existence of pyramidal acinar cells and prominent cellular borders with nearly smooth nuclear membrane. Well organized strands of RER were demarcated together with normal and some slightly blurred mitochondria. Numerous secretory granules and desmosomal junctions were obviously distinguished (Fig. 5a-d).

The basal membrane of ductal cells expressed clear infoldings with radial mitochondria. The nucleus appeared normal with few dispersed strands of RER. Abundant circumscribed granules were obvious with cellular interdigitations and desmosomes (Fig. 5e-h).

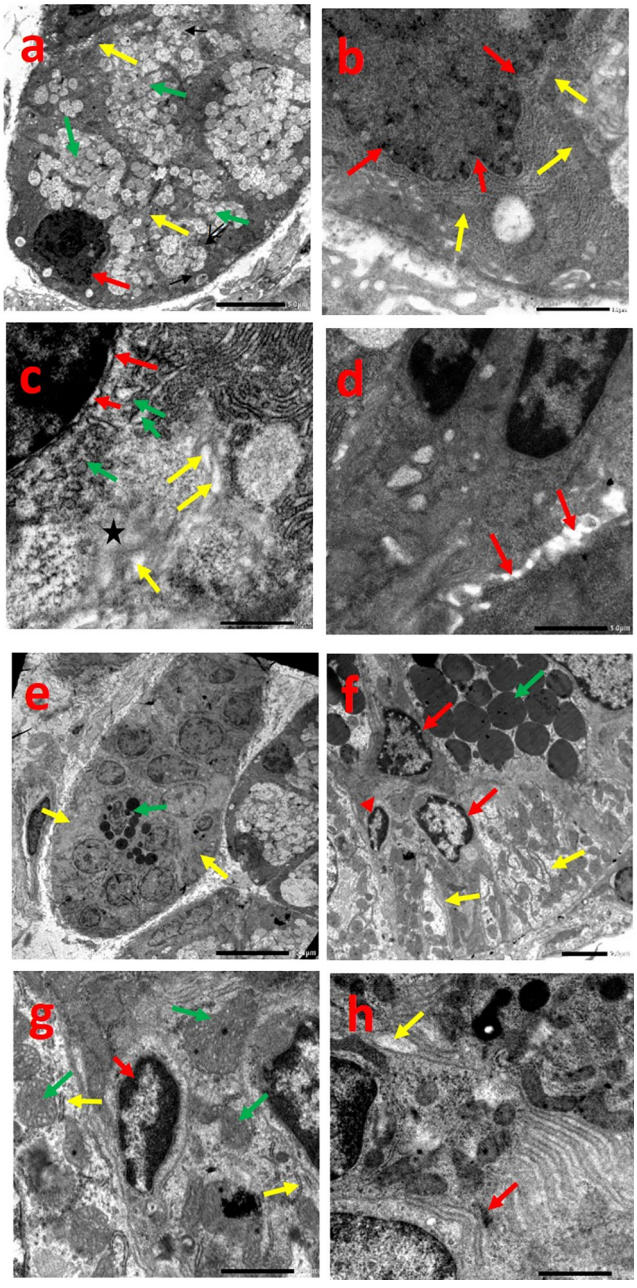

3.3. Masson's trichrome results

Group I showed thin rim of normally appearing deep blue collagen fibers surrounding the excretory duct. However, group II exhibited thick network configuration of fiber bundles encircling blood vessels and excretory ducts. Condensed rim of collagen fibers could be spotted in group III. In group IV, the excretory duct was bordered by apparently very thin rim of collagen bundles (Fig. 6a-d).

3.4. Immunohistochemical results

All groups revealed α SMA positive immunoreaction. Nevertheless, groups I and IV showed apparent increased positive reaction around the acini. Group III showed reduced reaction compared to the previous groups, while apparent minimal positive staining was detected in group II (Fig. 6e-h).

3.5. Statistical results

3.5.1. Area% of collagen

Statistically significant difference in area% of collagen was detected between groups I and II ($P < 0.001$) and between groups III and IV ($P < 0.001$), also when both were compared to group II ($P < 0.001$) (Fig. 6 i).

3.5.2. Area% of α SMA immunoreactivity

Statistically significant difference in area% of α SMA immunoreactivity was shown between groups I and II ($P < 0.001$), and when groups III and IV were compared to group II ($P < 0.001$). However, insignificant difference was detected between groups III and IV ($p = 0.867$) (Fig. 6 j).

4. Discussion

The submandibular gland was chosen due to its increased sensitivity to diabetic complications (Cheng et al., 2011).

Fig. 3 Electron micrograph of group II showing: acinar cells **(a-d)**, **(a)** irregular nuclear outline (red arrow), ill-defined shape of acinar & cellular boundaries (yellow arrows), fused irregular membrane bounded secretory granules (green arrows), **(b)** irregular nuclear indentations (red arrows), ill-defined mitochondria with blurred cristae (yellow arrows), **(c)** dilated nuclear membrane with perinuclear halo (red arrows), degenerated area (star), intracytoplasmic vacuolation (yellow arrows), dilated and fragmented RER (green arrows), **(d)** widened intercellular junctions with loss of desmosomal attachment (arrows) (Uranyl acetate and lead citrate (a)x1500, (b, c, d)x8000). Striated duct cells **(e-h)**, **(e)** indistinct basal infoldings (yellow arrows), sparse secretory granules (green arrow), **(f)** indistinct basal infoldings (yellow arrows), secretory granules (green arrow), irregular nuclei (red arrows), pyknotic nucleus (arrowhead), **(g)** pyknotic nucleus (red arrow), distended bizarre shaped mitochondria with disrupted cristae (green arrows), few disrupted RER (yellow arrows), **(h)** few desmosomal junctions (red arrow), widened intercellular spaces (yellow arrow) (Uranyl acetate and lead citrate (e)x800, (f)x2500, (g, h)x8000).

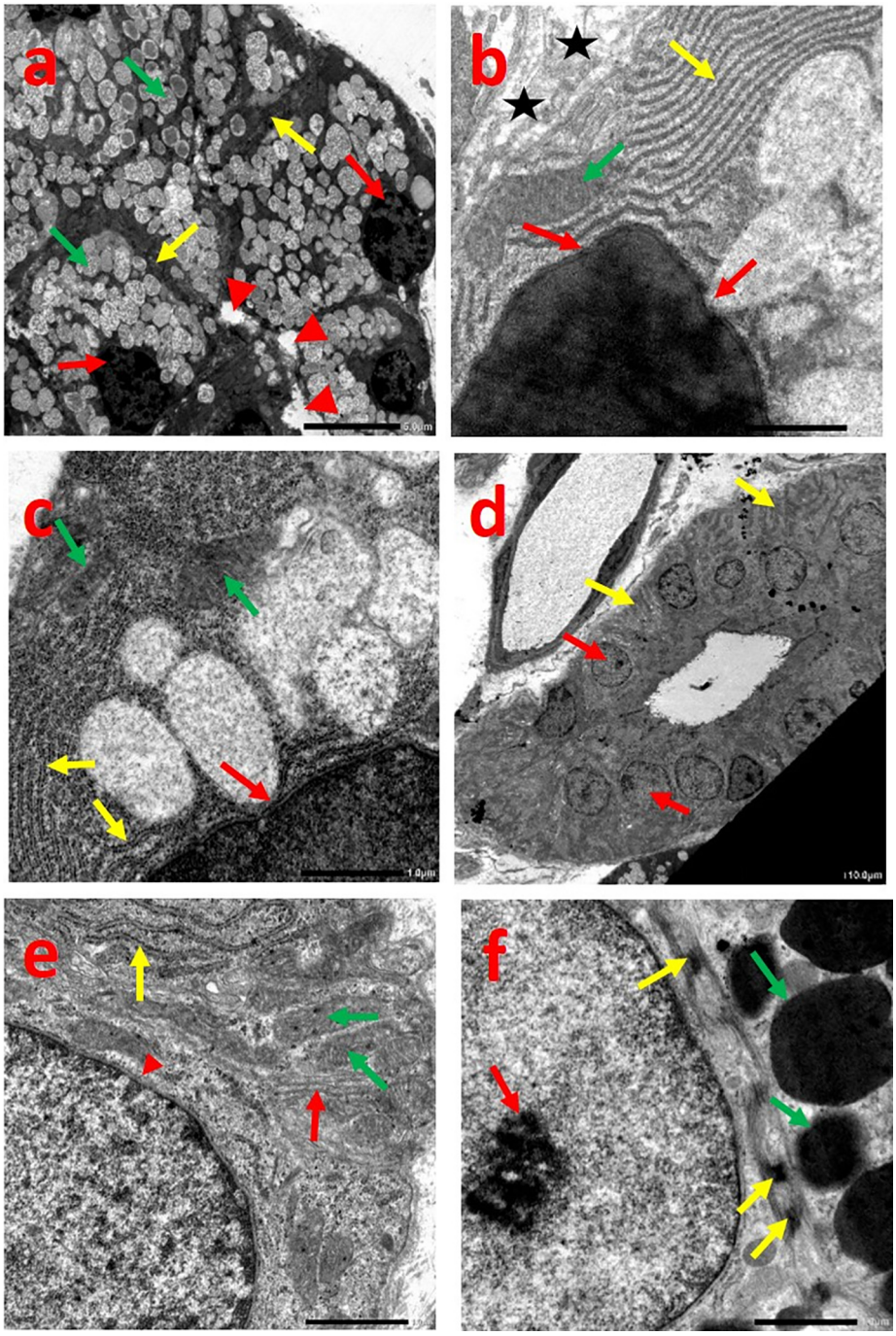

Fig. 4 Electron micrograph of group III showing: acinar cells **(a-c)**, **(a)** basal rounded nuclei (red arrows), definite cellular outlines (yellow arrows), vacuolar spaces (arrowheads), Abundant electron-lucent secretory granules (green arrows), **(b)** slight irregularity of nuclear membrane (red arrows), normal arrays of RER (yellow arrow), pleomorphic mitochondria (green arrow), disrupted cellular interdigitations and desmosomal junctions (stars), **(c)** slight irregularity of nuclear membrane (red arrows), normal arrays of RER (yellow arrows), ill-defined mitochondria (green arrows) (Uranyl acetate and lead citrate (a)x1500, (b, c)x8000). Striated duct cells **(d-f)**, **(d)** basal infoldings loaded with mitochondria (yellow arrows), rounded nuclei (red arrows), **(e)** regular nuclear membrane (arrowhead), few basal infolding (red arrow), elongated mitochondria (green arrows), scattered cisternae of RER (yellow arrow), **(f)** normal nucleus with prominent nucleolus (red arrow), secretory granules (green arrows), desmosomal junctions (yellow arrows) (Uranyl acetate and lead citrate (d)x800, (e, f)x8000).

Diabetes was induced by alloxan which aggravates destruction of beta cells of pancreas caused by reactive oxygen species (ROS), simulating type-1 DM (Ali, 2018).

Group II showed deterioration within the parenchymal elements in H&E stained sections and cellular organelles in TEM, which goes in agreement with several studies

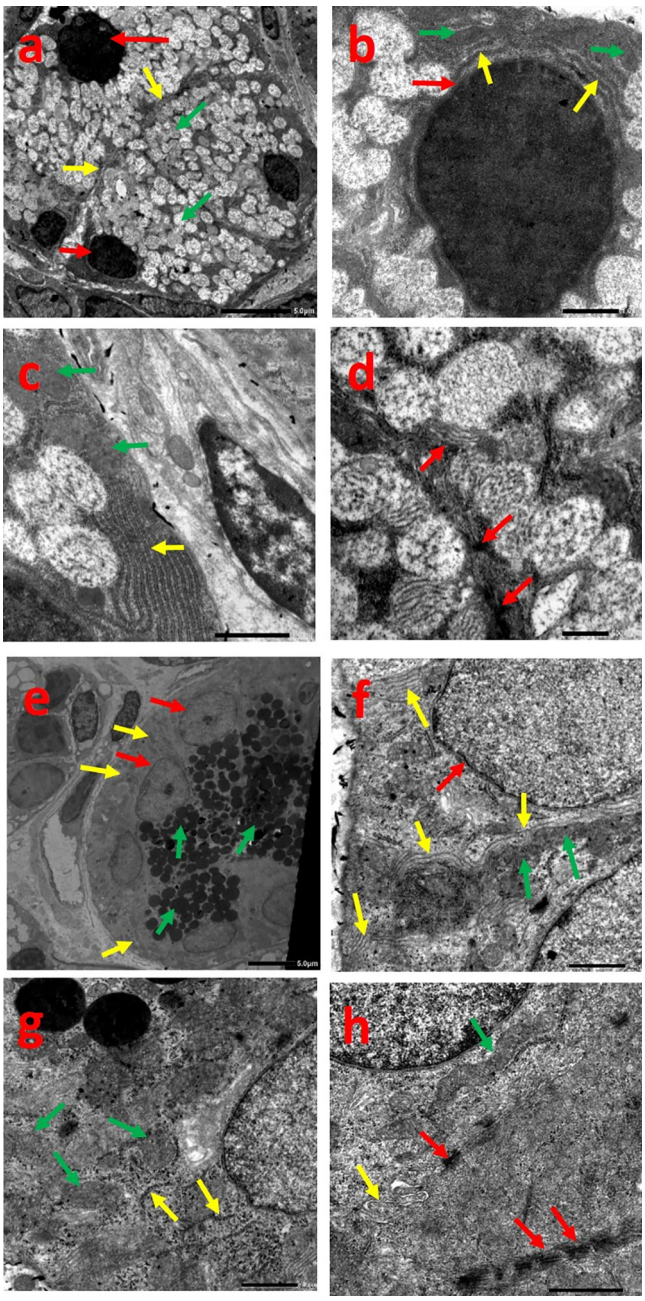

Fig. 5 Electron micrograph of group IV showing: acinar cells **(a-d)**, **(a)** basal rounded nuclei (red arrows), pyramidal cells and prominent cellular borders (yellow arrows), numerous secretory granules (green arrows), **(b)** smooth nuclear membrane (red arrow), strands of RER (yellow arrows), well defined mitochondria (green arrows), **(c)** well organized strands of RER (yellow arrow), slightly blurred mitochondria (green arrows), **(d)** normal desmosomal junctions (arrows) (Uranyl acetate and lead citrate (a)x1500, (b)x6000, (c)x8000, (d) x10000). Striated duct cells **(e-h)**, **(e)** basal infoldings loaded with mitochondria (yellow arrows), normal nuclei with prominent nucleolus (red arrows), numerous secretory granules (green arrows), **(f)** normal nuclear outline (red arrow), prominent basal infoldings (yellow arrows), radially arranged mitochondria (green arrows), **(g)** normal mitochondria (green arrows), dispersed strands of RER (yellow arrows), **(h)** elongated mitochondria (green arrow), cellular interdigitations (yellow arrow), desmosomal junctions (red arrows) (Uranyl acetate and lead citrate (e)x1000, (f, g)x6000, (h)x8000).

(Mahmoud & Mahmoud 2017; Al-Ankily et al., 2020; Elias, 2020; Salem et al., 2021). The recorded alterations verified that diabetes enhanced parenchymal destruction leading to induction of oxidative stresses (Sadeghinezhad et al., 2016). In addition, raised free fatty acids in diabetes may share in elevating ROS production. DNA fragmentation induces oxidative stresses allowing cellular damage and apoptotic death (El-Ghazawy et al., 2020).

The decreased cytoplasmic basophilia in group II acinar cells was suggested to be due to RER deficiency and disfigured mitochondrial cristae (Priyadi et al., 2019).

Atypical configuration of acinar and ductal cells observed in group II comes in agreement with Chen et al., 2020. This fact could be due to disruption of contractile proteins in the myoepithelial cells of diabetic rats (Shaker et al., 2017). However, ill-defined cellular outlines were concomitant with (El-Ghazawy et al., 2020). Potphode et al., 2018 reported that the free radicals formed in hyperglycemia produce abnormalities in the phospholipid bilayer of cell membranes which allows alteration in the bilayer properties (Rabea, 2017). Consequently, membrane rupture may occur due to increased permeability to ions initiating cell death (Potphode et al., 2018).

Cytoplasmic vacuolation observed in group II could be attributed to cellular accumulation of lipid which is dissolved during fixation and processing (Yasser & Shon, 2020).

The accumulation of coalesced secretory granules within the acinar cells in group II was in parallel with Chen et al., 2020; AbuBakr et al., 2020, which could be due to deficient contractility of myoepithelial cells. Another fact is that diabetes permits Ca^{2+} accumulation intracellularly sharing in reduction of gland function (El Sadik et al., 2018).

It's worthy to highlight that the striated duct of rat submandibular gland not only has role in electrolyte homeostasis, but also play a part in secretion of organic constituents (Tandler et al., 2001). This would clarify the existence of secretory granules within its cells in all groups.

NC was chosen as it is more efficient in lowering hyperglycemia compared to native curcumin (El-Far et al., 2017).

Groups III and IV manifested improvement in the parenchymal architecture with restoration of cellular configuration. These results come in accordance with other studies which recorded enhanced influence of NC on various tissues induced by different destructive stimuli (Sheibani et al., 2020; Kheiripour et al., 2021; Bulboacă et al., 2021).

It could be proposed that the potent curative effect of NC arises from its capability to manage the oxidative stress in DM by raising the action of main enzymes for the antioxidant defense (Maithilikarpagaselvi et al., 2016; Assis et al., 2017). Furthermore, curcumin can act by preventing p53 mediated mitochondrial Bax translocation (Ghosh et al., 2015). Curcumin may also be able to modulate the unfolded protein response signaling pathway in the RER (Afrin et al., 2015).

It is notable to emphasize that group IV exhibited, to some extent, better histological and ultrastructural features compared to group III. This was in close agreement with Abd El-Rahman & Al-Jameel, 2014 who documented that effectiveness of NC was enhanced in a dose dependent manner. Additionally, a dose of 200 mg/kg NC showed slightly better histological results than 100 mg/kg NC in treatment of induced ovarian and pancreatic defects in rats (Abuelezz et al., 2020).

Masson trichrome staining results were supported by statistical results showing increased collagen fiber deposition in

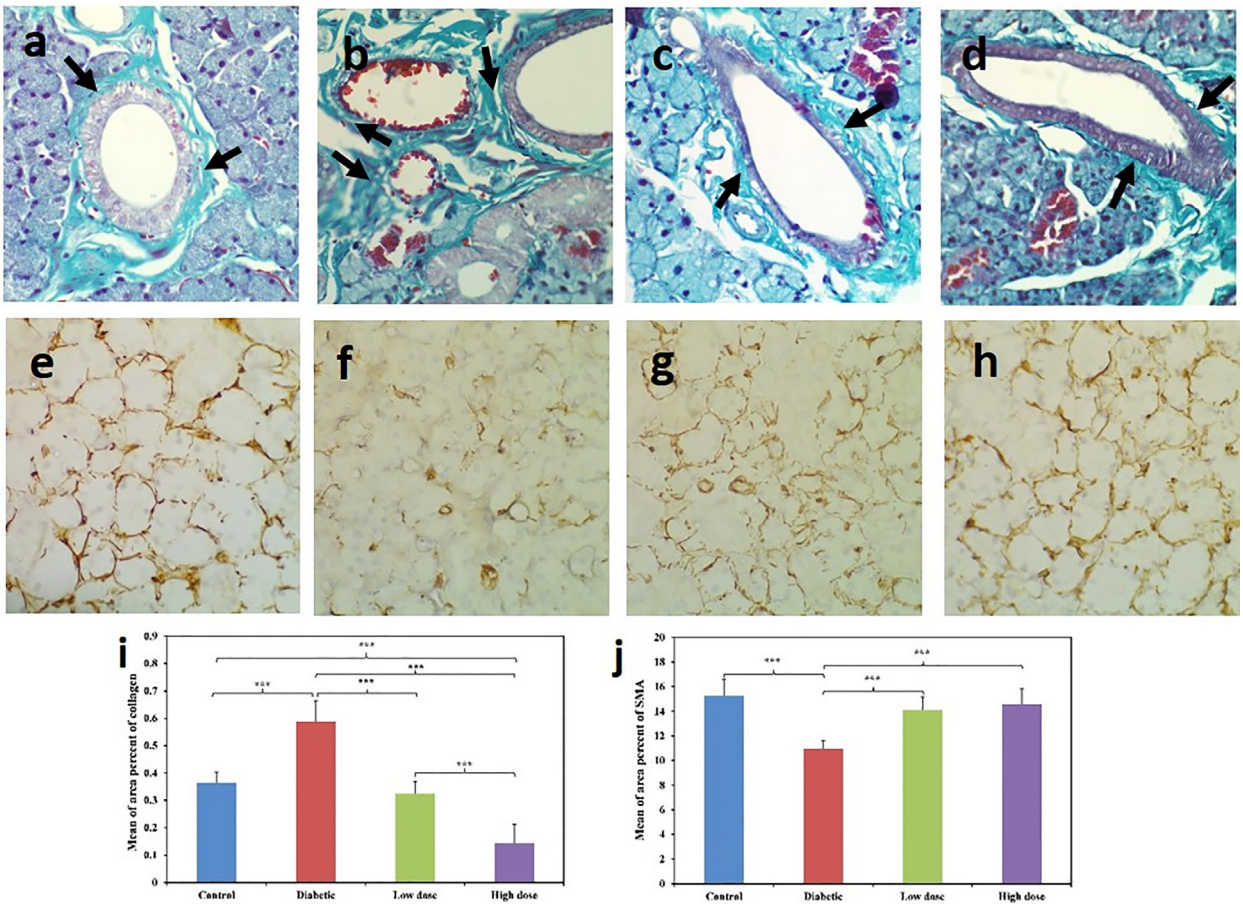

Fig. 6 Photomicrograph of rat submandibular gland showing: **(a) Group I;** thin rim of collagen fibers surrounding the excretory duct (arrows), **(b) Group II;** thick network of fiber bundles encircling the blood vessels and excretory duct (arrows), **(c) Group III;** condensed rim of collagen fibers (arrows), **(d) Group IV;** very thin rim of collagen fibers surrounding the excretory duct (arrows) (Masson Trichromex400). **(e) Group I, (h) Group IV;** extensive positive brown immunostained cells, **(f) Group II;** minimal positive brown immunostained cells, **(g) Group III;** some positive brown immunostained cells (α SMA x400). **(i)** bar chart showing values of means and SD for area % of collagen between the studied groups. *** $P < 0.001$, **(j)** bar chart showing values of means and SD for area % of α SMA immunoreactivity between the studied groups. *** $P < 0.001$.

group II and reduction in the treated groups. This was reinforced by El-sharkawy et al., 2018 and Sudirman et al., 2019 who clarified fibrosis encircling the excretory ducts of submandibular glands and kidney fibrosis in diabetic rats. This could be attributed to hyperglycemia which causes disordered remodeling activity of fibroblasts (Monteiro et al., 2017). Several studies proved that NC reduced fibrosis in induced hepatotoxicity and diabetic rats' kidneys (Ismaiel et al., 2015; Sudirman et al., 2019). NC could suppress fibroblast proliferation and collagen synthesis (Kazemi-Darabadi et al., 2019).

α SMA marker was found to detect the degree of myoepithelial cell proliferation (El Sadik et al., 2018). The immunoreaction showed apparent increased reaction in all groups except the diabetic group, which was supported by statistical analysis. Similar results were proved by El Sadik et al., 2018 who spotted minor reaction of α SMA in the offspring of diabetic rats' mothers, verifying alterations in the submandibular glands' development.

5. Conclusion

NC profoundly rescued the induced diabetic histopathological and ultrastructural alterations of the submandibular gland highlighting its antioxidant potentiality in a dose dependent manner. Yet, the obtained results put forward an inspiring base for future formulation advances on a range of doses to attain the most superior dose.

Funding

This research did not receive any specific grant from funding agencies in the public, commercial, or not-for-profit sectors.

Ethical statement

The experimental design was permitted by the Research Ethics Committee of Faculty of Dentistry, Minia University (Decision No. 509).

CRediT authorship contribution statement

Maha El Shahawy: Conceptualization, Data curation, Formal analysis, Funding acquisition, Investigation, Methodology, Project administration, Resources, Supervision, Validation,

Visualization, Writing – original draft, Writing – review & editing. **Mona El Deeb:** Conceptualization, Data curation, Formal analysis, Funding acquisition, Investigation, Methodology, Project administration, Resources, Supervision, Validation, Visualization, Writing – original draft, Writing – review & editing.

Declaration of Competing Interest

The authors declare that they have no known competing financial interests or personal relationships that could have appeared to influence the work reported in this paper.

Appendix A. Supplementary data

Supplementary data to this article can be found online at https://doi.org/10.1016/j.sdentj.2022.04.009.

References

Abd Elhameed, M., 2018. The effect of (cod liver oil-insulin) combination on suppressing the diabetes deleterious effect on the excretory ducts of sublingual salivary glands of albino rats. EDJ 64 (1), 233–248.

Abd El-Rahman, S., Al-Jameel, S., 2014. Efficacy of nano curcumin in F-2 isoprostanes in male rats treated with Cisplatin and Methotrexate as chemotherapy drugs. IJSR 4 (2), 157–179.

AbuBakr, N., Haggag, T., Sabry, D., Salem, Z., 2020. Functional and histological evaluation of bone marrow stem cell-derived exosomes therapy on the submandibular salivary gland of diabetic Albino rats through TGFβ/ Smad3 signaling pathway. Heliyon 6, (4) e03789.

Abuelezz, N., Shabana, M., Abdel-Mageed, H., Rashed, L., Morcos, G., 2020. Nanocurcumin alleviates insulin resistance and pancreatic deficits in polycystic ovary syndrome rats: Insights on PI3K/AkT/mTOR and TNF-α modulations. Life Sci. 256, 118003.

Afrin, R., Arumugam, S., Soetikno, V., Thandavarayan, R., Pitchaimani, V., Karuppagounder, V., Sreedhar, R., Harima, M., Suzuki, H., Miyashita, S., Nomoto, M., Suzuki, K., Watanabe, K., 2015. Curcumin ameliorates streptozotocin-induced liver damage through modulation of endoplasmic reticulum stress-mediated apoptosis in diabetic rats. Free Radic. Res. 49 (3), 279–289.

Al-Ankily, M., Shamel, M., Bakr, M., 2020. Epidermal Growth Factor Improves the Ultrastructure of Submandibular Salivary Glands of Streptozotocin Induced Diabetic Rats - A Qualitative Study. Int. J. Medi. Dental Sci. 9 (1), 1803–1810.

Ali, S., 2018. Stereological and immunhistochemical study on the submandibular gland of diabetic albino rats. J. Am. Sci. 14 (12), 24–33.

Araghi, A., Nazaktabar, A., Sayrafi, R., Salehi, A., Golshahi, H., Jahanbakhsh, M., Seifi, S., 2017. The Effects of in ovo Nanocurcumin Administration on Oxidative Stress and Histology of Embryonic Chicken Heart. Poultry Sci. J. 5 (2), 105–111.

Assis, R., Arcaro, C., Gutierres, V., Oliveira, J., Costa, P., Baviera, A., Brunetti, I., 2017. Combined effects of curcumin and lycopene or bixin in yoghurt on inhibition of LDL oxidation and increases in HDL and paraoxonase levels in streptozotocin-diabetic rats. Int. J. Mol. Sci. 18, 332.

Aziz, N., Wal, A., Wal, P., Pal, R., 2019. Preparation and Evaluation of the Polyherbal Powder: The Nature's Pharmacy for the Treatment of Diabetes Mellitus and Its Complications. Pharmacophores 10 (1), 60–70.

Bansal, S., Goel, M., Aqil, F., Vadhanam, M., Gupta, R., 2011. Advanced drug delivery systems of curcumin for cancer chemoprevention. Cancer Prev. Res. 4 (8), 1158–1171.

Bulboacă, A., Porfire, A., Bolboacă, S., Nicula, C., Feştilă, D., Roman, A., Râjnoveanu, R., Râjnoveanu, A., Dogaru, G., Boarescu, P., Rus, V., Bulboacă, C., Bulboacă, A., Stănescu, I., 2021. Protective Effects of Liposomal Curcumin on Oxidative Stress/Antioxidant Imbalance, Metalloproteinases 2 and -9, Histological Changes and Renal Function in Experimental Nephrotoxicity Induced by Gentamicin. Antioxidants (Basel) 10 (2), 325.

Chen, S., Wang, Y., Zhang, C., Yang, Z., 2020. Decreased basal and stimulated salivary parameters by histopathological lesions and secretory dysfunction of parotid and submandibular glands in rats with type 2 diabetes. Exp. Ther. Med. 19 (4), 2707–2719.

Cheng, S., Wu, V., Kwong, D., Ying, M., 2011. Assessment of post-radiotherapy salivary glands. Br. J. Radiol. 84, 393–402.

Cui, F., Hu, M., Li, R., Li, B., Huang, D., Ma, W., Jia, X., Lv, Z., 2021. Insulin on changes in expressions of aquaporin-1, aquaporin-5, and aquaporin-8 in submandibular salivary glands of rats with Streptozotocin-induced diabetes. Int. J. Clin. Exp. Pathol. 14 (2), 221–229.

El Sadik, A., Mohamed, E., El Zainy, A., 2018. Postnatal changes in the development of rat submandibular glands in offspring of diabetic mothers: Biochemical, histological and ultrastructural study. PLoS ONE 13, (10) e0205372.

El-Far, Y., Zakaria, M., Gabr, M., El Gayar, A., Eissa, L., El-Sherbiny, I., 2017. Nanoformulated natural therapeutics for management of streptozotocin-induced diabetes: potential use of curcumin nanoformulation. Nano-medicine 12, 1689e711.

El-Ghazawy, Y., El-Zainy, M., Hassan, R., 2020. Histological and Immunohistochemical Analysis of Green Coffee Aqueous Extract Effect on Parotid Salivary Gland in Streptozotocin Induced Diabetic Albino Rats. EJH. 43 (3), 748–762.

Elias, W., 2020. The Anti-Diabetic Effect of Hibiscus Cannabinus Extract on the Submandibular Salivary Gland of Alloxan-Induced Diabetic Albino Rats. Int. J. Pharmaceutical Res. Allied Sci. 9 (2), 195–202.

El-sharkawy, R., El-kammar, H., Obeid, R., Bdelkhalek, A., 2018. Effects of moringa oleifera aqueous leaf extract on submandibular salivary glands of diabetic albino rats. EDJ 64 (2), 1293–1303.

Estakhri, M., Shokrzadeh, M., Jaafari, M., Karami, M., Mohammadi, H., 2019. Organ toxicity attenuation by nanomicelles containing curcuminoids: Comparing the protective effects on tissues oxidative damage induced by diazinon. Iran J Basic Med. Sci. 22, 17–24.

Ghosh, S., Bhattacharyya, S., Rashid, K., Sil, P., 2015. Curcumin protects rat liver from streptozotocin-induced diabetic pathophysiology by counteracting reactive oxygen species and inhibiting the activation of p53 and MAPKs mediated stress response pathways. Toxicol. Rep. 2, 365–376.

Gouda, W., Hafiz, N., Mageed, L., Alazzouni, A., Khalil, W., Afify, M., Abdelmaksoud, M., 2019. Effects of nano-curcumin on gene expression of insulin and insulin receptor. Bull. National Res. Centre 43 (128), 1–10.

Ismaiel, A., El-Denshary, E., El-Nekeety, A., Al-Yamani, M., Gad, A., Hassan, N., Abdel-Wahhab, M., 2015. Ameliorative Effects of Curcumin Nanoparticles on Hepatotoxicity Induced by Zearalenone Mycotoxin. Global J. Pharmacol. 9 (3), 234–245.

Kato, M., Nishikawa, S., Ikehata, A., Dochi, K., Tani, T., Takahashi, T., Imaizumi, A., Tsuda, T., 2017. Curcumin improves glucose tolerance via stimulation of glucagon-like peptide-1 secretion. Mol. Nutr. Food Res. 61, 16.

Kazemi-Darabadi, S., Nayebzadeh, R., Shahbazfar, A., Kazemi-Darabadi, F., Fathi, E., 2019. Curcumin and Nanocurcumin Oral Supplementation Improve Muscle Healing in a Rat Model of Surgical Muscle Laceration. Bull. Emerg. Trauma 7 (3), 292–299.

Keirnan, J., 2015. Histological and histochemical methods, theory and practice. Scion Publishing Limited Press p:, pp. 184–206.

Kheiripour, N., Plarak, A., Heshmati, A., Asl, S., Mehri, F., Ebadollahi-Natanzi, A., Ranjbar, A., Hosseini, A., 2021. Evaluation of the hepatoprotective effects of curcumin and nanocurcumin against paraquat-induced liver injury in rats: Modulation of

oxidative stress and Nrf2 pathway. J Biochem. Mol. Toxicol. 35, (5) e22739.

Maciejczyk, M., Kossakowska, A., Szulimowska, J., Klimiuk, A., Knaś, M., Car, H., Niklińska, W., Robert, J., Chabowski, A., Zalewska, A., 2017. Lysosomal Exoglycosidase Profile and Secretory Function in the Salivary Glands of Rats with Streptozotocin-Induced Diabetes. J. Diabetes Res. https://doi.org/10.1155/2017/9850398.

Mahmoud, E., Mahmoud, M., 2017. Effect of Pomegranate Peel Extract on Submandibular Salivary Glands of Streptozotocin-Induced Diabetes in Rats: Histological, Immunohistochemical and Ultrastructural Study. J. Adv. Biol. Biotechnol. 13 (3), 1–15.

Maithilikarpagaselvi, N., Sridhar, M., Swaminathan, R., Zachariah, B., 2016. Curcumin prevents inflammatory response, oxidative stress and insulin resistance in high fructose fed male Wistar rats: potential role of serine kinases. Chem. Biol. Interact. 244, 187–194.

Monteiro, M., D'Epiro, T., Bernardi, L., Fossati, A., Santos, M., Lamers, M., 2017. Long- and short-term diabetes mellitus type1 modify young and elder rat salivary glands morphology. Arch. Oral Biol. 73, 40–47.

Potphode, N., Daunde, J., Desai, S., Walvekar, M., 2018. Nano-curcumin: A potent enhancer of body antioxidant system in diabetic mice. L. Int. J. Phytomed. 10 (3), 162–167.

Pourghasem, M., Nasiri, E., Shafi, H., 2014. Early renal histological changes in alloxan-induced diabetic rats. Int. J. Mol. Cell Med. 3, 11–15.

Prasad, S., Gupta, S., Tyagi, A., Aggarwal, B., 2014. Curcumin, a component of golden spice: from bedside to bench and back. Biotechnol. Adv. 32 (6), 1053–1064.

Priyadi, A., Muhtadi, A., Suwantika, A., Sumiwi, S., 2019. An economic evaluation of diabetes mellitus management in South East Asia. J. Adv. Pharm. Educ. Res. 9 (2), 53–74.

Rabea, A., 2017. Comparative study on the possible effect of cod liver oil versus insulin on parotid salivary glands of streptozotocin-induced diabetic albino rats. EDJ 63, 439–467.

Ranjbar, A., Gholami, L., Ghasemi, H., Kheiripour, N., 2020. Effects of nano-curcumin and curcumin on the oxidant and antioxidant system of the liver mitochondria in aluminum phosphide-induced experimental toxicity. Nanomed. J. 7 (1), 58–64.

Sadeghinezhad, J., Tootian, Z., Javadi, F., 2016. Anatomical and histological structure of the tongue and histochemical characteristics of the lingual salivary glands in the Persian squirrel (Sciurus anomalus). Anat. Sci. Int. 93 (1), 58–68.

Salem, Z., Kamel, A., AbuBakr, N., 2021. Salivary exosomes as a new therapy to ameliorate diabetes mellitus and combat xerostomia and submandibular salivary glands dysfunction in diabetic rats. J. Mol. Histol. 52 (3), 467–477.

Shaker, W., Taha, R., Ghali, L., 2017. Effect of Bone Marrow-Derived Stem Cells on the Submandibular Salivary Glands of Streptozotocin-induced Diabetic Rats. Suez Canal University Medical Journal 20 (1), 29–37.

Shamsi-Goushki, A., Mortazavi, Z., Mirshekar, M., Mohammadi, M., MoradiKor, N., Maskouni, S., Shahraki, M., 2020. Comparative Effects of Curcumin versus Nano-Curcumin on Insulin Resistance, Serum Levels of Apelin and Lipid Profile in Type 2 Diabetic Rats. Diabetes, Metabolic Syndrome and Obesity: Targets and Therapy 13, 2337–2346.

Sheibani, M., Dehpour, A., Nezamoleslami, S., Mousavi, S., Jafari, M., Sorkhabadi, S., 2020. The protective effects of curcumin and curmumin nanomicelle against cirrhotic cardiomyopathy in bile duct-ligated rats. Nanomed. J. 7 (2), 158–169.

Sudirman, S., Lai, C., Yan, Y., Yeh, H., Kong, Z., 2019. Histological evidence of chitosan-encapsulated curcumin suppresses heart and kidney damages on streptozotocin-induced type-1 diabetes in mice model. Sci. Rep. 9 (1), 15233, 2019.

Taiema, D., Saleh, R., Deraz, E., 2019. Effect of ozone on submandibular salivary gland of alloxan-induced diabetic rats: Histological and ultrastructural study. Life Sci. J. 16 (10), 112–121.

Tandler, B., Gresik, E., Nagato, T., Phillips, C., 2001. Secretion by striated ducts of mammalian major salivary glands: review from an ultrastructural, functional, and evolutionary perspective. Anat. Rec. 264 (2), 121–145.

Yasser, S., Shon, A., 2020. Histomorphometric and Immunohistochemical Study Comparing the Effect of Diabetes Mellitus on the Acini of the Sublingual and Submandibular Salivary Glands of Albino Rats. Macedonian J. Med. Sci. 8, 49–54.

Ye, M., Qiu, H., Cao, Y., Zhang, M., Mi, Y., Yu, J., Wang, C., 2017. Curcumin Improves palmitate-induced insulin resistance in human umbilical vein endothelial cells by maintaining proteostasis in endoplasmic reticulum. Front. Pharmacol. 8, 148.